Met. Mater. Int., Vol. 23, No. 2 (2017), pp. 369~377
doi: 10.1007/s12540-017-6417-2

Strength of Cu-28 wt%Ag Composite Solidified Under High Magnetic Field Followed by Cold Drawing

Congcong Zhao[1,2], Xiaowei Zuo[1,3], Engang Wang[1,3,*], and Ke Han[4,*]

[1]Key Laboratory of Electromagnetic Processing of Materials (Ministry of Education), Northeastern University, Shenyang 110819, China
[2]School of Materials Science and Engineering, Northeastern University, Shenyang 110819, China
[3]School of Metallurgy, Northeastern University, Shenyang 110819, China
[4]National High Magnetic Field Laboratory, Florida State University, Tallahassee 32310, FL, USA

(received date: 21 June 2016 / accepted date: 7 September 2016)

Cu-Ag composite is one of the best conductors for high-field magnets. Increasing its strength is crucial for designing newer high-field magnets. Cu-28 wt%Ag samples were solidified with and without a 12-T high magnetic field (HMF), and then cold-drawn. We investigated the influence of HMF on microstructure, hardness and strength of Cu-Ag samples both before and after cold-drawing. The introduction of external HMF during solidification increased both the dendrite arm spacing and the dissolved Ag in Cu, and it reduced the spacing between both the Ag precipitates in proeutectic Cu and the eutectic lamellae. The transversal microstructure after cold-drawing inherited the network solidification structure, but at a refined scale. The Cu dendrite spacing in the 12-T HMF samples at all deformation strain was larger than that without HMF. HMF slightly increased the intensity of <111> fiber texture of Cu, which strengthened proeutectic Cu at the level of 3.5 deformation strain. In samples deformed to strain of 3.5, refined Ag precipitation spacing, increased Ag solubility in Cu matrix, and refined eutectic lamellar spacing by 12-T HMF increased the strength by 5% in the sample compared with that without HMF.

Keywords: composites, high magnetic field, solidification, tensile test, precipitation

1. INTRODUCTION

Currently, most available high-strength conductor materials are metal-metal composites, such as Cu-Ag, Cu-Nb, and Cu-Be composites, which can be used to build high-field magnets [1-3]. High strength is required to resist strong Lorentz forces occurring in high field, while high electrical conductivity is needed to suppress Joule heating [4-6]. An ultimate tensile strength (UTS) of 700 MPa and an electrical conductivity of 75% IACS (International Annealed Copper Standard) are required to advance high-field Bitter magnets [7]. Cu (Face-Centered-Cubic, FCC) -Nb (Body-Centered-Cubic, BCC) alloy and Cu-Ag (FCC-FCC) alloy are two of the best materials for high-field magnets [5,6,8,9]. Compared with Cu-Ag alloy, the large difference of the melting temperature between Cu and Nb makes it difficult to fabricate large-size ingots. Sakai *et al.* [10] and Benghalem and Morris [11] indicated that the strength increased with Ag content and tended to saturate beyond 16-30 wt%Ag. On the other hand, the electrical conductivity showed a reverse tendency with increasing Ag content [10]. Cu-Ag alloys with about 24-30 wt%Ag became the most promising candidates because of the excellent combination of strength and electrical conductivity.

In order to achieve high-strength and high-conductivity, plastic deformation and heat treatment were applied to Cu-Ag alloys [2,12-16]. Severe plastic deformation processes, such as cold drawing [17,18], cold rolling [7,19,20], high-pressure torsion [21], and equal channel angular pressing [22,23], were used to refine the microstructure and to increase the strength. The solubility of Cu in Ag is 8.8 wt% at the eutectic temperature (779 °C), and that of Ag in Cu is 8 wt%. The solubility limits are low at room temperature. Because of the low solubility at room temperature, Ag precipitates were formed during the solid transformation of Cu-Ag alloy. Both discontinuous and continuous precipitation modes of Ag were observed [24-27]. By optimizing the cold working and thermomechanical process, Sakai *et al.* [10] have reported Cu-Ag composites with strength of 1000 MPa and conductivity of 80% IACS. A UTS of 1050 MPa and a conductivity of 75% IACS were realized in Cu-24 wt%Ag sheet [7].

Hypoeutectic Cu-Ag composites contain two components: proeutectic Cu matrix embedded with Ag precipitates and eutectics consisting of Cu and Ag phases [13,28]. The Cu-Ag

*Corresponding authors: egwang@mail.neu.edu.cn, han@magnet.fsu.edu

composites, with high Ag concentration, showed a two-stage hardening during the cold-working process [10,11]. During the first stage, because of the large scale of both proeutectic Cu matrix and eutectic component, the total strength of the alloy could be determined by the rule of mixture of the two components [11,13,15,29]. The Hall-Petch equation was capable of estimating the strength of each component, which meant that the initial scale of the microstructure (both eutectic and Ag precipitation in the Cu matrix) in Cu-Ag alloy was very important to change the strength. Several ways were used to improve the initial microstructure, such as adding a third element [25,27,30,31], applying both directional solidification [32-35] and external magnetic fields [28,36-38]. During the second stage, Ag precipitates became too fine to maintain an internal dislocation structure. The work hardening of Cu matrix and eutectics, the grain-boundary strengthening, and the strengthening of Ag fibers should be considered individually to the total strength of Cu-Ag alloy [11].

External high magnetic field (HMF) applied during solidification was proved to modify the microstructure of several alloys [39-43], and also for Cu-Ag alloy [28,36,38]. Moreau *et al.* [44,45] indicated that HMF suppressed the natural convection of the melt by introducing a Lorentz force, and also produced a new thermoelectromagnetic convection (TEMC). Previous work [28,35,36] showed that the microstructure and properties of Cu-Ag alloys could be change by introducing an external HMF during the solidification process. The Ag precipitates in Cu matrix played an important role to the total strength of Cu-Ag alloy. In order to refine the spacing of Ag precipitates, we applied 12-T HMF during the solidification processing of Cu-28 wt%Ag alloy in this work. The microstructural evolution was investigated in both as-cast and as-drawn Cu-Ag samples. The strengthening mechanisms were established to explain the enhancement in strength under HMF in the terms of solid solution strengthening, precipitation strengthening, and texture strengthening.

2. EXPERIMENTAL PROCEDURES

Cu-28 wt%Ag alloy was prepared with high-purity Ag bars (99.996 wt%) and oxygen-free Cu bars (99.97 wt%) in an intermediate-frequency vacuum induction furnace under high-purity Ar atmosphere. The machined and polished samples (9 mm in diameter and 65 mm in length) were placed in a high-purity graphite crucible and then sealed with a quartz tube. The sealed sample was placed in the center of a vacuum resistance furnace under a high-field superconducting magnet, which can generate a magnetic field with a maximum magnetic flux density of 12-T at the center of a Φ100 mm cold bore. The central points of the samples were coincided with the center of the high magnetic field and the vacuum furnace. The samples were heated to 1323 K with a heating rate of 5 K/min, held for 40 mins for homogeneity, then cooled to room temperature with the average rate of 15 K/min. During the solidification process, we used magnetic flux density B of 0-T and 12-T to investigate the influence of high magnetic field on the solidification structure of Cu-28 wt%Ag alloy.

Afterwards, the Cu-28 wt%Ag alloy rods were drawn at ambient temperature at a deformation strain given by $\varepsilon = \ln(A_0/A)$, where A_0 and A are the initial and final cross-sectional area. The maximum ε was 3.5. No intermediate annealing was applied during the drawing process.

The transverse and longitudinal sections of the solidified and drawn samples were polished and etched in a solution of $FeCl_3$, HCl and C_2H_5OH. The microstructure was examined by SZX16 optical microscope, SSX-550 scanning electron microscope (SEM), Zeiss 1540 XB field emission scanning electron microscopy (FESEM), and JEOL-2011 transmission electron microscopy (TEM). The weight percent of Ag in Cu matrix was measured by Energy Dispersive X-ray Spectrometer (EDS) in SEM. Samples for TEM were prepared by grinding a 3-mm diameter disk to about 30 μm in thickness, and then argon ion-milling at 5 kV. Microhardness tests were performed using a diamond indenter under a load of 0.3 kg for a dwelling time of 10 s. Tensile tests were performed at a rate of 1 mm/min with the tensile axes parallel to the drawing direction. The crystal structures of Cu phase and Ag phase in selected as-cast and drawn samples ($\varepsilon = 1.4$, $\varepsilon = 2.4$) with and without a 12-T magnetic field were analyzed by X-ray diffraction (XRD) on the longitudinal sectioned samples.

3. RESULTS

3.1. Microstructure evolution

The microstructure of Cu-28 wt%Ag alloy consists of two components (Fig. 1): Cu-rich proeutectic dendrite (dark contrasts) and eutectic component (light contrasts), which forms a network surrounding Cu-rich dendrites. The dendrite arm spacing is increased (Table 1) by HMF, because it suppresses the convection and increases the Ag solute concentration in front of the solid/liquid interface during the growth of dendrites, restraining the nucleation of new Cu dendrites [36].

HMF reduces the inter-lamellar spacing of eutectic (Table 1). The inter-lamellar spacing is proportional to the solute diffusion coefficient in the liquid [46], and the diffusion coefficient. With the application of HMF, the diffusion coefficient decreases as B^{-4} or B^{-2} (B, the magnetic flux density of the applied magnetic field) with the applied magnetic field [47], decreasing the inter-lamellar spacing of eutectic. In previous work [28], where 12T-HMF was also superimposed when Cu-28 wt%Ag alloy was in molten status and 30-min-holding close to eutectic temperature, the inter-lamellar spacing of eutectic in 12-T HMF sample was larger than that in 0-T sample. More homogeneous solute distribution in liquid melt was expected in the 30-min-holding sample than that without. As a result, the undercooling for the nucleation of eutectic

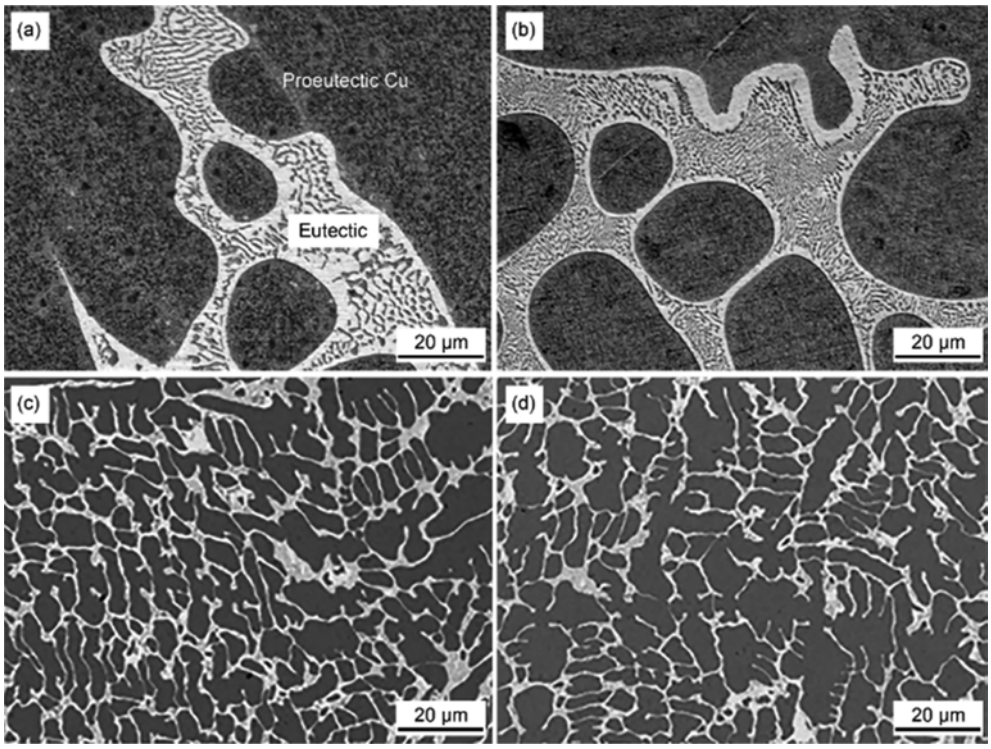

Fig. 1. Longitudinal microstructure of as-cast Cu-28 wt%Ag alloy solidified with (a) 0-T HMF and (b) 12-T HMF; transversal microstructure of as-drawn Cu-28 wt%Ag composite ($\varepsilon = 3.5$) after solidifying with (c) 0-T HMF and (d) 12-T HMF.

Table 1. Microstructural characterizations of as-cast Cu-28 wt%Ag alloys solidified with and without a 12-T HMF

Applied HMF	Mean Cu dendrite spacing (μm)	Mean eutectic lamellar spacing (μm)	Ag content in Cu matrix (wt%)	Volume fraction of eutectics (%)
0-T	33±0.7	1.7±0.13	7.1±0.4	28±2
12-T	35±0.6	1.2±0.05	8.2±0.5	29±2

was larger, leading to a higher temperature gradient (∇T). The temperature gradient produced a Seebeck electromotive force $S\nabla T$, where S is the thermoelectric power of the material. If the gradients of S and T were not parallel, a thermoelectric current (TE) was generated. The interaction between the TE current and the magnetic field produced a thermoelectric magnetic force and TEMC developed in the vicinity of the interface on the microscopic scale [41]. With higher temperature gradient, the TEMC might be more significant in the 30-min-holding sample during the growth of eutectic. The TEMC may induce the short-range to long-range transition of the solute diffusion. As a consequence, the inter-lamellar of eutectic in 30-min-holding sample was increased with the application of 12-T HMF.

Ag content in Cu matrix detected by SEM-EDS, which includes both the Ag precipitation and the solid solute Ag in Cu, in 12-T HMF sample is higher than that in 0-T sample. The equilibrium partition coefficient, $k = C_S^*/C_L^*$, where C_S^* and C_L^* are respectively the solid and liquid concentration at the solid/liquid interface, was not changed by the application of 12-T magnetic field according to previous work [36]. The Ag content in Cu matrix increased because of the increased Ag concentration in front of the solid/liquid interface. Finally, HMF is incapable of changing the shape of the network (Fig. 1(a) and (b) and the volume fraction of eutectic (Table 1).

As-cast Cu-28 wt%Ag alloy was drawn to wires without any heat treatment. The transverse-sectional eutectic network is still remained after deformation, as shown in Figs. 1(c) and (d). Because they have cube-on-cube orientation relationship and same slip systems [48,49], Cu and Ag with FCC crystallographic structures have good compatibility during deformation. Cu dendrites on longitudinal sections are drawn into long strip morphology, and the eutectic component is likewise elongated (Fig. 2). Fibrous structure begins to form parallel to the drawing direction when deformation strain reaches about 2.4. The dendrite spacing in the 12-T sample is larger than that without HMF at every deformation strain (Fig. 2(e)). The evolution of transvers-sectional microstructure and dendrite spacing during the deformation indicates the heredity

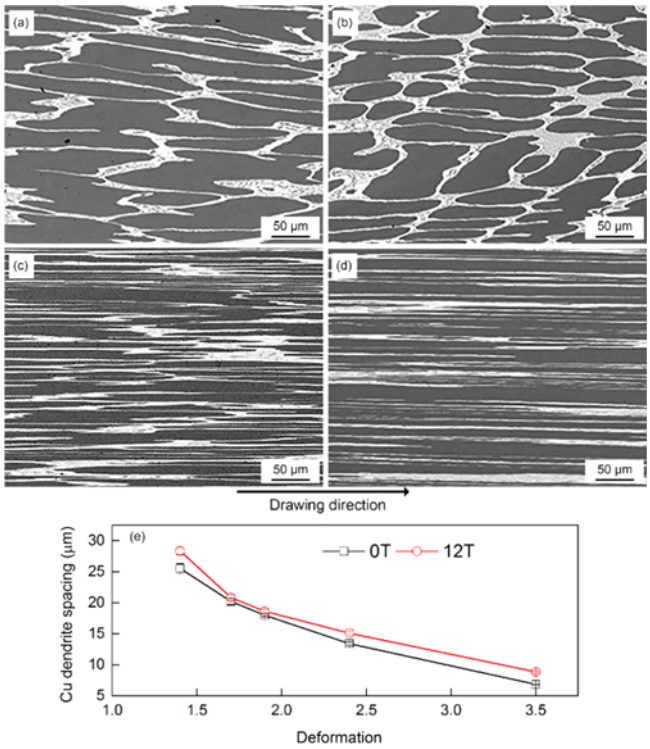

Fig. 2. Longitudinal microstructure of as-drawn Cu-28 wt%Ag composite after solidifying without a 12-T HMF: (a) $\varepsilon = 1.4$; (b) $\varepsilon = 3.5$, and with a 12-T HMF: (c) $\varepsilon = 1.4$; (d) $\varepsilon = 3.5$. (e) The dendrite spacing plotted as a function of deformation rate.

of microstructure from as-cast state to drawn state. A relationship of the spacing between as-drawn and as-cast samples was fitted as a function of drawing strain by the formula

$$\lambda_1 = \lambda_0 e^{-0.5s} \quad (1)$$

where λ_1, λ_0, and ε are the spacing of as-drawn sample, the spacing of as-cast sample, and drawing strain, respectively [28].

Nanosized Ag precipitates are observed in proeutectic Cu matrix of as-drawn Cu-Ag composite, as shown in Fig. 3. Two kinds of spacing between Ag precipitates are shown on transvers sections: the spacing of precipitate rows and the spacing of precipitate particles, which was similar to the distribution of Ag precipitation in aged Cu-8 wt%Ag alloy [26]. We individually measured the two kinds of spacing. T-test, which could be used to determine if two sets of data were significantly different from each other, was used to identify the difference between the spacing of precipitates without and with a 12-T HMF. According to the t-test result (at the level of 0.05), the spacing of precipitate rows is insignificantly different in two samples, however, the spacing of precipitate particles in 12-T sample is significantly smaller than that in 0-T sample, as shown in Table 2. The reason for the two kind of spacing was related to the formation position of

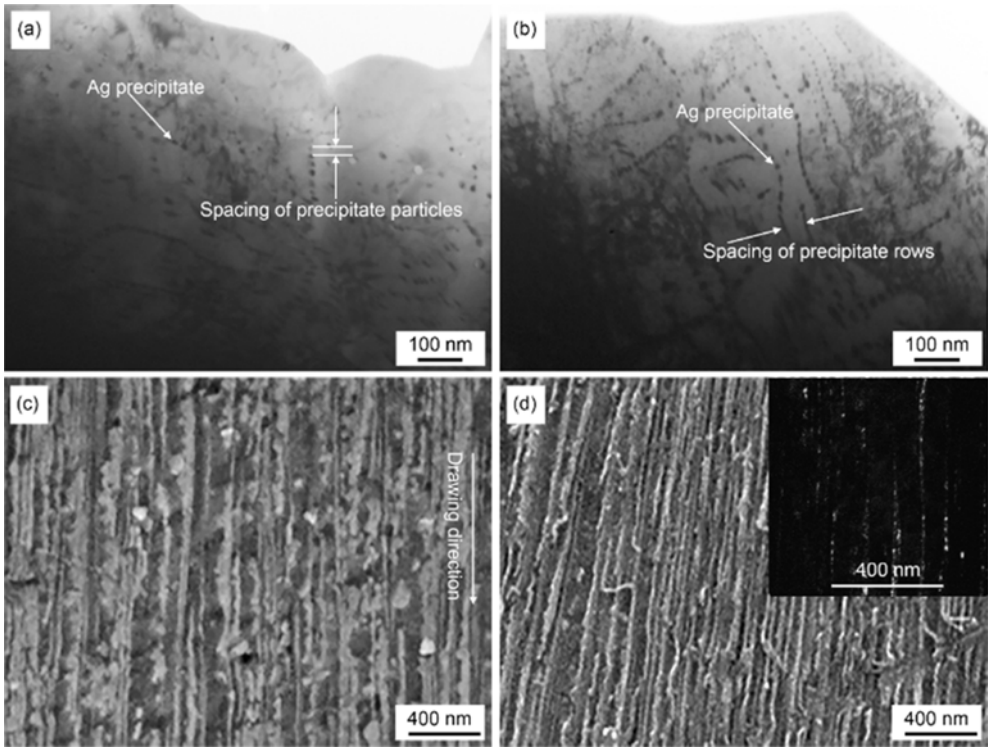

Fig. 3. Transversal TEM images of Ag precipitation in proeutectic Cu matrix of the as-drawn Cu-28 wt%Ag composite ($\varepsilon = 3.5$) after solidifying (a) without and (b) with a 12-T HMF. The morphology of Ag precipitation in Cu matrix of drawn alloy ($\varepsilon = 3.5$) in the longitudinal section (c) without and (d) with a 12-T HMF. The inset in (d) is the dark field image of longitudinal section showing Ag fibers drawn from Ag precipitation.

Table 2. Mean center-to-center spacing between Ag precipitates in as-drawn Cu-28 wt%Ag composite ($\varepsilon = 3.5$)

	Spacing between precipitate particles	Spacing between precipitate rows
0-T alloy	24.7±4.5 nm	48.7±11.7 nm
12-T alloy	17.6±2.0 nm	49.3±14.2 nm
T-test (0.05)	Significant	Not significant

Ag precipitated out of Cu matrix. Disc-shaped Ag precipitates within Cu matrix were observed in the {100} planes in single crystals of a Cu-5.7 wt%Ag alloy after 400-640 °C heat treatment [50]. Two kinds of spacings, the spacing of precipitates on the same plane and the spacing of precipitates on different plane, can be observed, when the precipitates form in a certain plane.

The microstructure heredity from the as-cast state to the drawn state indicated that both eutectic lamellar spacing and Ag precipitate spacing should have a consistent tendency formulated by Eq. 1 between the as-cast state and the drawn state. Therefore, eutectic lamellar spacing in drawn Cu-28 wt%Ag with a 12-T HMF should be smaller than that without a 12-T HMF. According to Eq. 1 and the measured spacing of Ag precipitate particles in as-drawn samples, the spacing in as-cast samples are calculated as 142 nm and 101 nm for 0-T and 12-T samples, which indicates that the spacing of Ag precipitate particles in 12-T as-cast sample is much smaller than that in 0-T as-cast. The spacing of Ag precipitate rows is about 282 nm for both kinds of alloys. Ag precipitation spacing is much smaller than the scales of both proeutectic Cu dendrite spacing and the inter-lamellar spacing of eutectic.

3.2. X-ray Results

The XRD intensity of the Cu phase (Fig. 4(a)) is much higher than that of the Ag phase because of the higher volume fraction of Cu in the alloy. The normalized results show that HMF enhances the intensity of (111) diffraction peaks of both Cu and Ag, but reduces the intensity of (220) diffraction peaks in as-cast alloy. This means that the [111] crystal direction tends to tilt along the direction of HMF, which is consistent with the results on the directionally solidified Al-0.85 wt%Cu alloy at low growth speech under a high magnetic field [51]. The surface tension of the cellular and dendritic tip was the main reason for the deflection of primary dendrite arm from the solidification and resulting in orienting the [111] direction of Cu along the magnetic direction. Moreover, (220) diffraction peaks become the strongest peaks in both Cu and Ag phases in the as-drawn sample with the deformation rate of 2.4. In as-drawn samples (Fig. 4(b) and (c)), inverse pole figures show that <111> and <001> duplex fiber texture parallel to the drawing direction are observed. Cu and Ag are both FCC structure, and they have

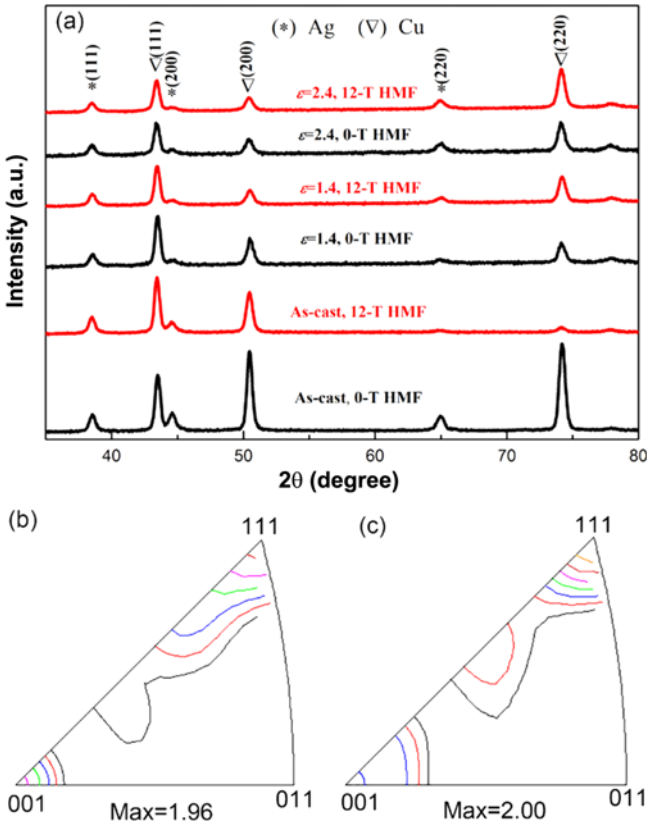

Fig. 4. (a) XRD results of as-cast and drawn ($\varepsilon = 1.4$, $\varepsilon = 2.4$) Cu-28 wt%Ag alloy solidified with and without a 12-T high magnetic field. Inverse pole figures (IPFs) of Cu matrix along drawing direction of as-drawn Cu-28 wt%Ag composite ($\varepsilon = 2.4$) after solidifying with (b) 0-T HMF, and (c) 12-T HMF.

the same slip system, {111}<110> (the close-packed plane and close-packed direction). The slip system tended to rotate toward drawn direction during the cold drawing, which caused the increased intensity of (220) and <111> fiber texture. With the application of 12-T HMF, the intensity of <111> fiber texture slightly increases while the intensity of <001> fiber texture component decreases.

3.3. Strength and hardness of Cu-28 wt%Ag composite

The hardness and tensile strength of Cu-28 wt%Ag composite after solidifying without and with a 12-T HMF, shown in Fig. 5, indicate that the strength of as-drawn samples increases as the increasing deformation strain because of the refinement of microstructure by the drawing (Fig. 2). The strength of 12-T HMF sample is larger than that of 0-T HMF sample at every deformation strain. At the deformation strain of 3.5, the hardness and strength of the alloy solidified under a 12-T HMF increases by 7% and 5% than without HMF. The increase should be related to the decreased Ag precipitates spacing, eutectic inter-lamellar spacing and increased Ag in Cu, which would be discussed in details later.

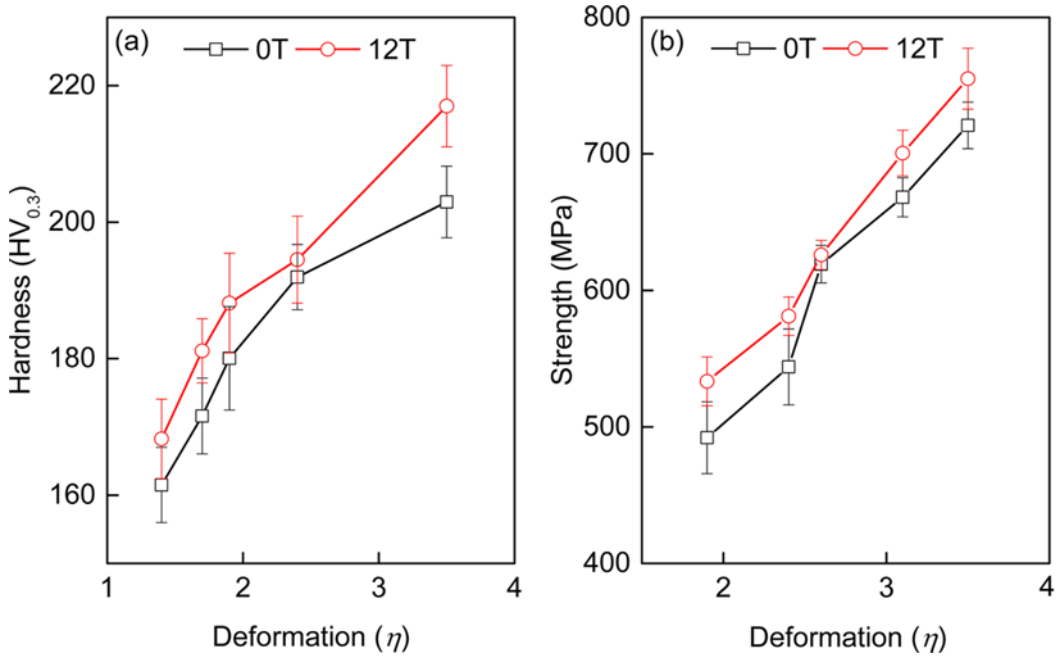

Fig. 5. (a) Hardness and (b) ultimate tensile strength (UTS) of Cu-28 wt%Ag composite as a function of deformation rate.

4. DISCUSSION

4.1. Effect of HMF on the spacing of Ag precipitation

According to the morphology of Ag precipitates (shown in 3(a) and (b)) and the previous works [25,26], the Ag precipitates in Cu-28 wt%Ag alloy were continuous precipitates, which nucleated inside the grains. Higher supersaturated Ag content in Cu matrix, caused by the application of 12-T HMF, brought larger driving force for the nucleation. The above results also showed that the spacing of spherical Ag precipitates in 12-T HMF sample was smaller than that in 0-T HMF sample. The increased driving force for the nucleation and smaller spacing of Ag precipitate resulted in the increased hardness and strength. In previous work [28], where 30-min-holding was applied during the solidification process, the spacing of Ag precipitate in 12-T HMF sample was also smaller than that in 0-T sample in as-cast sample. In as-drawn samples of previous work [28], however, the spacing of Ag precipitates in 12-T HMF sample was larger than that in 0-T sample, which was the main reason for the decrease in strength after applying the HMF.

4.2. Enhancement in strength of as-drawn Cu-Ag composite under HMF

The strength of Cu-Ag alloy can be calculated using the rule of mixture because of the large scale of both proeutectic Cu matrix and eutectic component, and the Hall-Petch relationship can be used to determine the strength of the proeutectic Cu and eutectic regions. Moreover, the solid solution Ag atoms have different atomic size and shear modulus from the matrix, which brought into solid solution strengthening to Cu matrix. The strength of Cu-28 wt%Ag alloy (σ) can be described by [13,25]:

$$\sigma = (1-V_{eut})\left[\sigma_{0(Cu)}+k_{Cu/Ag}\lambda_{0Ag,precip}^{-\frac{1}{2}}\exp(\varepsilon/4)+k\sqrt{\frac{x_a}{3}}\right] V_{eut}\left[\sigma_{0(Ag)}+k_{eut}\lambda_{0eut}^{-\frac{1}{2}}\exp(\varepsilon/4)\right] \quad (2)$$

where V_{eut} is the volume fraction of the eutectic, $\sigma_{0(Cu)}$ is the strength of pure Cu, $k_{Cu/Ag}$ is the strengthening coefficient for proeutectic Cu matrix (the strengthening coefficient for pure Cu was used), $\lambda_{0Ag,\ precip.}$ is the Ag precipitates spacing in Cu matrix in as-cast alloys, k is a function of alloying element and lattice parameter change due to added elements, and x_a is the Ag atomic fraction with the solid solution in Cu, $\sigma_{0(Ag)}$ is the strength of pure Ag, k_{eut} is the strengthening coefficient for eutectic component (the strengthening coefficient for pure Ag was used), λ_{0eut} is the inter-lamellar spacing of eutectic component in as-cast alloys, ε is the deformation strain. k in Eq. 2 can be calculated using the equation [25],

$$k = G(|\delta| + 1/20|\eta|)^{3/2} \quad (3)$$

where G is the shear modulus of matrix (G_{Cu} = 46 GPa and G_{Ag} = 30 GPa), δ = 0.1302 is a factor of lattice change, η = 0.3485 is a factor describing the change of the shear modulus due to alloying. G for 0-T sample was calculated as 45.9 GPa with 0.6 at% Ag, and 45.8 GPa for 12-T sample with 1 at% Ag dissolved in Cu matrix. The averaged values of the two

Table 3. Modelling parameters used in Eq. 2 and individual contributions to the total strength of Cu-28 wt%Ag composite at the deformation strain of 3.5

	0-T alloy	12-T alloy
Strength of pure Cu, $\sigma_{0(Cu)}$ (MPa) [52]	20	20
$k_{Cu/Ag}$ (MPa$\sqrt{m}$) [52]	0.14	0.14
Average Ag precipitates spacing, $\lambda_{0Ag,\,precip}$ (nm)	211	193
k	2605	2596
Calculated Ag solubility in Cu, x_a (at%)	0.6%	1%
Strength of pure Ag, $\sigma_{0(Ag)}$ (MPa) [52]	37.3	37.3
k_{eut} (MPa$\sqrt{m}$) [52]	0.068	0.068
Precipitation strengthening, $\varepsilon = 3.5$	526	543
Solid solution strengthening, $\varepsilon = 3.5$	84	106
Eutectic strengthening, $\varepsilon = 3.5$	35	43

kinds of Ag precipitates spacing, which were measured in the as-drawn sample with a deformation strain of 3.5, were used to calculate the precipitates spacing in as-cast alloy by Eq. 1. The volume fraction of Ag precipitates is 5.2% and 5.6% for the samples without and with HMF, respectively. The Ag solubility in Cu matrix was determined by subtracting the volume fraction of Ag precipitates from the Ag content in Cu matrix detected by SEM-EDS (Table 1). The parameters used in Eq. 2 and calculated results are shown in Table 3.

The calculated strength according to Eq. 2 and the measured strength of Cu-Ag alloys without and with a 12-T HMF as a function of deformation strain are plotted in Fig. 6(a). The results show that the calculated results are consistent with the measured strength, especially at low deformation strain. The strength of Cu-Ag alloy consists of five parts, as shown in Fig. 6(b). The strength of Cu and Ag, and the solid solution strengthening are not change with the deformation. The precipitation strengthening and the strength of eutectic increase with increasing deformation strain. The precipitation strengthening accounts for 70%-79% of the total strength.

In the presence of the HMF during the solidification of Cu-Ag alloy, the increased Ag solubility in Cu, decreased Ag precipitates spacing, and refined inter-lamellar spacing in eutectic in the as-cast sample increased the strength of Cu-Ag composite eventually.

5. CONCLUSIONS

(1) HMF during solidification of Cu-28 wt%Ag alloy increased the dendrite arm spacing, and trapped additional Ag in proeutectic Cu, but it reduced the eutectic lamellar spacing and the spacing between Ag precipitate particles.

(2) The Cu dendrite spacing of as-drawn Cu-28 wt%Ag composite after solidifying with 12-T HMF was larger than that without HMF, which was inherited from the as-cast microstructure. The additional Ag trapped in Cu matrix with the application of 12-T HMF increased the nucleation rate of Ag precipitation, consequently decreasing the Ag precipitation spacing.

(3) The application of HMF enhanced the intensity of (111) diffraction peaks, but reduced the intensity of (220) diffraction peaks in as-cast Cu-28 wt%Ag alloy. HMF marginally increased the intensity of <111> fiber texture of Cu, but decreased the intensity of <001> fiber texture in as-drawn alloys.

(4) The strength was increased in Cu-Ag composite that was solidified under a 12-T magnetic field followed by cold drawing because of the refined Ag precipitation spacing,

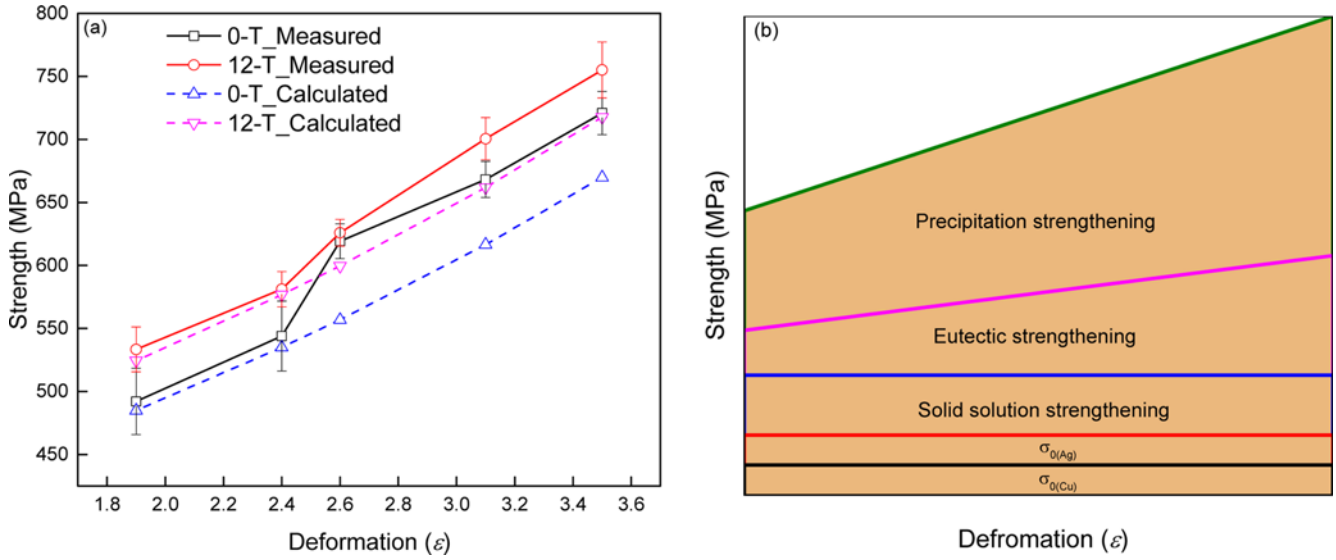

Fig. 6. (a) Measured and calculated values of the strength at various deformation strain, (b) Schematic illustration of strengthening effect from individual parts in Cu-Ag alloys.

increased Ag solubility in Cu matrix, and refined inter-lamellar spacing in eutectic component. The precipitation strengthening played an important role in the total strength.

ACKNOWLEDGEMENT

This work was supported by the National Natural Science Foundation of China (Nos. 51474066 and 51004038), and the 111 Project of China (No. B07015). A portion of this work was performed at the National High Magnetic Field Laboratory (NHMFL), which is supported by National Science Foundation Cooperative Agreement No. DMR-1157490 and the State of Florida. The authors are grateful to Dr. Yan Xin and Dr. Rongmei Niu at NHMFL for assisting with the microstructure characterization. The authors are also thankful to Dr. Mary Tyler for editing.

REFERENCES

1. J. Bevk, J. P. Harbison, and J. L. Bell, *J. Appl. Phys.* **49**, 6031 (1978).
2. T. Hirota, A. Imai, T. Kumano, M. Ichihara, Y. Sakai, H. Maeda, *et al. IEEE T. Magn.* **30**, 1891 (1994).
3. T. Asano, Y. Sakai, M. Oshikiri, K. Inoue, H. Maeda, F. Herlach, *et al. IEEE T. Magn.* **30**, 2106 (1994).
4. D. Dew-Hughes, *Mat. Sci. Eng. A* **168**, 35 (1993).
5. K. Han, A. Baca, H. Coe, J. Embury, K. Kihara, H. J. Schneider-Muntau, *et al. IEEE T. Appl. Supercon.* **10**, 1277 (2000).
6. W. Grünberger, M. Heilmaier, and L. Schultz, *Physica B* **294-295**, 643 (2001).
7. Y. Sakai, K. Inoue, and H. Maeda, *Acta Metall. Mater.* **43**, 1517 (1995).
8. L. Deng, K. Han, B. Wang, X. Yang, and Q. Liu, *Acta Mater.* **101**, 181 (2015).
9. S. I. Hong, M. A. Hill, Y. Sakai, J. T. Wood, and J. D. Embury, *Acta Metall. Mater.* **43**, 3313 (1995).
10. Y. Sakai, K. Inoue, T. Asano, and H. Maeda, *IEEE T. Magn.* **28**, 888 (1992).
11. A. Benghalem and D. G. Morris, *Acta Mater.* **45**, 397 (1997).
12. K. Han, V. J. Toplosky, R. Goddard, L. Jun, R. M. Niu, and J. P. Chen, *IEEE T. Appl. Supercon.* **22**, 6900204 (2012).
13. K. Han, A. A. Vasquez, Y. Xin, and P. N. Kalu, *Acta Mater.* **51**, 767 (2003).
14. Y. Sakai and H. J. Schneider-Muntau, *Acta Mater.* **45**, 1017 (1997).
15. S. I. Hong and M. A. Hill, *Acta Mater.* **46**, 4111 (1998).
16. W. B. Lee, E. H. Yoon, and S. B. Jung, *J. Mater. Sci. Lett.* **22**, 1751 (2003).
17. K. Han, J. D. Embury, J. R. Sims, L. J. Campbell, H. J. Schneider-Muntau, V. I. Pantsyrnyi, *et al. Mat. Sci. Eng. A* **267**, 99 (1999).
18. S. I. Hong and M. A. Hill, *Mat. Sci. Eng. A* **264**, 151 (1999).
19. Y. G. Ko, S. Namgung, B. U. Lee, and D. H. Shin, *J. Alloy. Compd.* **504**, S448 (2010).
20. C. A. Davy, H. Ke, P. N. Kalu, and S. T. Bole, *IEEE T. Appl. Supercon.* **18**, 560 (2008).
21. Y. Z. Tian, X. H. An, S. D. Wu, Z. F. Zhang, R. B. Figueiredo, N. Gao, *et al. Scripta Mater.* **63**, 65 (2010).
22. Y. Z. Tian, W. Z. Han, H. J. Yang, S. X. Li, S. D. Wu, and Z. F. Zhang, *Scripta Mater.* **62**, 183 (2010).
23. F. H. Latief and S. I. Hong, *Met. Mater. Int.* **21**, 746 (2015).
24. A. T. Adorno, M. R. Guerreiro, and R. A. G. Silva, *Mat. Sci. Eng. A* **374**, 170 (2004).
25. J. Freudenberger, J. Lyubimova, A. Gaganov, H. Witte, A. L. Hickman, H. Jones, *et al. Mat. Sci. Eng. A* **527**, 2004 (2010).
26. C. C. Zhao, X. W. Zuo, E. G. Wang, R. N. Niu, and K. Han, *Mat. Sci. Eng. A* **652**, 296 (2016).
27. A. Gaganov, J. Freudenberger, E. Botcharova, and L. Schultz, *Mat. Sci. Eng. A* **437**, 313 (2006).
28. X. W. Zuo, K. Han, C. C. Zhao, R. N. Niu, and E. G. Wang, *Mat. Sci. Eng. A* **619**, 319 (2014).
29. Y. Z. Tian, J. J. Li, P. Zhang, S. D. Wu, Z. F. Zhang, M. Kawasaki, *et al. Acta Mater.* **60**, 269 (2012).
30. J. B. Liu, L. Zhang, A. P. Dong, L. T. Wang, Y. W. Zeng, and L. Meng, *Mat. Sci. Eng. A* **532**, 331 (2012).
31. D. Raabe and D. Mattissen, *Acta Mater.* **46**, 5973 (1998).
32. Z. P. Que, J. H. Lee, H. M. Jung, J. H. Shin, S. Z. Han, and K. J. Euh, *J. Cryst. Growth* **362**, 58 (2013).
33. K. Liu, Z. Jiang, J. Zhao, J. Zou, Z. Chen, and D. Lu, *J. Alloy. Compd.* **612**, 221 (2014).
34. X. W. Zuo, G. Rui, B. L. An, L. Zhang, and E. G. Wang, *Acta Metall. Sinica* **52**, 143 (2016).
35. X. W. Zuo, R. Guo, C. Zhao, L. Zhang, E. Wang, and K. Han, *J. Alloy. Compd.* **676**, 46 (2016).
36. X. W. Zuo, C. C. Zhao, E. G. Wang, L. Zhang, K. Han, and J. C. He, *J. Low Temp. Phys.* **170**, 409 (2013).
37. X. W. Zuo, C. C. Zhao, R. M. Niu, E. G. Wang, and K. Han, *J. Mater. Process. Tech.* **224**, 208 (2015).
38. P. Lehmann, R. Moreau, D. Camel, and R. Bolcato, *J. Cryst. Growth* **183**, 690 (1998).
39. Z. H. I. Sun, X. Guo, M. Guo, J. Vleugels, O. Van der Biest, and B. Blanpain, *J. Alloy. Compd.* **551**, 568 (2013).
40. X. Li, Z. Ren, Y. Fautrelle, Y. Zhang, and C. Esling, *Mater. Lett.* **64**, 2597 (2010).
41. X. Li, Z. Ren and Y. Fautrelle, *J. Cryst. Growth* **310**, 3488 (2008).
42. X. W. Zuo, E. G. Wang, H. Han, L. Zhang, and J. C. He, *J. Alloy. Compd.* **492**, 621 (2010).
43. Y. D. Zhang, C. Esling, M. Calcagnotto, M. L. Gong, X. Zhao, and L. Zuo, *J. Phys. D Appl. Phys.* **40**, 6501 (2007).
44. R. Moreau, O. Laskar, M. Tanaka, and D. Camel, *Mat. Sci. Eng. A* **173**, 93 (1993).
45. R. Moreau, *Prog. Cryst. Growth Ch.* **38**, 161 (1999).
46. D. A. Porter, K. E. Easterling, and M. Sherif, *Phase Transformations in Metals and Alloys*, 3rd ed., pp.153-188, Chapman and Hall, London, UK (1981).

47. V. Botton, P. Lehmann, R. Bolcato, R. Moreau, and R. Haettel, *Int. J. Heat Mass Tran.* **44**, 3345 (2001).
48. J. B. Liu, L. Meng, and Y. W. Zeng, *Mat. Sci. Eng. A* **435-436**, 237 (2006).
49. D. W. Yao and L. Meng, *Physica B* **403**, 3384 (2008).
50. R. Monze, K. Murase, H. Nagayoshi, and C. Watanabe, *Phil. Mag. Lett.* **84**, 349 (2004).
51. X. Li, Y. Fautrelle, and Z. Ren, *Acta Mater.* **56**, 3146 (2008).
52. J. H. Schneibel and M. Heilmaier, *Mater. Trans.* **55**, 44 (2014).